

Magnetic neutron star equilibria with stratification and type-II superconductivity

S. K. Lander^{1,2*}, N. Andersson¹ and K. Glampedakis³

¹ *Mathematical Sciences, University of Southampton, Southampton SO17 1BJ, U.K.*

² *Max-Planck-Institut für Gravitationsphysik, Albert-Einstein-Institut, Potsdam-Golm 14476, Germany*

³ *Theoretical Astrophysics, University of Tübingen, Auf der Morgenstelle 10, Tübingen 72076, Germany*

15 February 2018

ABSTRACT

We construct two-fluid equilibrium configurations for neutron stars with magnetic fields, using a self-consistent and nonlinear numerical approach. The two-fluid approach — likely to be valid for large regions of all but the youngest NSs — provides us with a straightforward way to introduce stratification and allows for more realistic models than the ubiquitous barotropic assumption. In all our models the neutrons are modelled as a superfluid, whilst for the protons we consider two cases: one where they are a normal fluid and another where they form a type-II superconductor. We consider a variety of field configurations in the normal-proton case and purely toroidal fields in the superconducting case. We find that stratification allows for a stronger toroidal component in mixed-field configurations, though the poloidal component remains the largest in all our models. We provide quantitative results for magnetic ellipticities of NSs, both in the normal- and superconducting-proton cases.

Key words: stars: neutron, stars: magnetic fields, MHD, stars: magnetars

1 INTRODUCTION

It has long been acknowledged that neutron stars (NSs) have strong magnetic fields, which may play a variety of roles in the physics of these objects. Magnetic fields can change the stability of a NS, affect its evolution and cooling properties, induce precession and provide the restoring force for a class of oscillation modes (Harding & Lai 2006; Mereghetti 2008). They may also produce crust-core coupling and affect the post-glitch spin behaviour of NSs (Easson 1979; Dib, Kaspi & Gavril 2008). All of these effects are likely to be sensitive to the details of the magnetic-field configuration in the stellar interior, whereas we are only able to observe the exterior, dominantly dipolar, field. For this reason considerable effort has gone into modelling the interior magnetic fields of neutron stars; we give an overview of this in section 2.

Despite considerable progress, the vast majority of studies on magnetised neutron stars treat them as barotropic single-fluid bodies. Whilst this is a sensible way to begin producing simplified models, more realistic studies need to confront some of the detailed interior physics of NSs. For example, over forty years since the first predictions that neutron star matter would contain superfluid neutrons and superconducting protons (see, e.g., Baym, Pethick & Pines (1969)), there have been no attempts to construct multifluid magnetic equilibria along these lines. The issue is highly topical, too — recent observations of the cooling of the young NS in Cassiopeia A are well explained by a model with superfluid neutrons and superconducting protons (Shternin et al. 2011; Page et al. 2011). In the case of no magnetic field there has been more progress, including studies of the equilibria and oscillation modes of superfluid NSs (e.g. Prix & Rieutord (2002); Prix, Novak & Comer (2005); Yoshida & Eriguchi (2004); Passamonti, Haskell & Andersson (2009)). The closest related work on magnetised stars is probably the study of *single-fluid* barotropic NSs with superconductivity, by Akgün & Wasserman (2008).

A simpler problem than a NS with superfluidity/superconductivity is a stratified (i.e. non-barotropic), magnetised star composed of normal fluid. Stratification is expected to exist in NSs (Reisenegger & Goldreich 1992), where it can allow for

* skl@soton.ac.uk

a wider range of equilibrium configurations as well as providing a stabilising effect on the magnetic field (Reisenegger 2009). Again, the limitations of barotropic stellar models have been known for decades (Mestel 1956), but there have been few attempts to construct stratified magnetised equilibria. Most of the work in this direction has been that of Braithwaite and collaborators, who perform nonlinear magnetohydrodynamics (MHD) evolutions of a stratified star and show that the system appears to relax to an equilibrium over time (Braithwaite & Nordlund 2006; Braithwaite 2009). In addition, Mastrano et al. (2011) very recently studied single-fluid non-barotropic models of NSs, albeit using pre-specified magnetic field configurations.

In this paper we attempt to plug some of the gaps in the literature, presenting the first results for magnetised NS equilibria modelled as a two-fluid system. We treat the neutrons as being a superfluid, which mainly interacts with the proton fluid through the star’s gravitational potential. By choosing different degrees of compressibility for the two fluid species, we can introduce stratification. We begin by considering the case where protons are a magnetised normal fluid and find equilibria with purely poloidal, purely toroidal and mixed-field configurations. After this, we treat the ‘full’ problem where the neutron star is composed of superfluid neutrons and type-II superconducting protons for the first time, specialising to the case of a purely toroidal magnetic field. This paper takes a nonlinear approach to the problem, but we have also worked on a separate study using perturbation theory; the results of this are presented in a parallel paper, Glampedakis, Andersson & Lander (2011).

This paper is laid out as follows. In section 2 we present the equilibrium equations for our stellar model, independent of the details of the magnetic field. We then specialise to the case where the protons are a normal fluid governed by standard MHD. In section 3 we consider the case where the protons are instead a type-II superconductor, presenting simplified equations which nonetheless are likely to be accurate enough for an initial study of equilibria. In the case of purely toroidal fields we derive equations in a form suitable for numerical integration. In section 4 we give details of our numerical procedure, whilst in section 5 we show how to convert code output (in terms of dimensionless code variables) into useful physical quantities. Section 6 contains our results for two-fluid equilibria, exploring the effect of stratification and type-II superconductivity and section 7 is a discussion.

2 TWO-FLUID EQUILIBRIUM EQUATIONS AND NORMAL MHD

2.1 Equilibrium equations for two-fluid magnetic stars

We begin by modelling a neutron star as axisymmetric, with the magnetic symmetry axis being the same as the rotation axis. For this system it is natural to use cylindrical polar coordinates (ϖ, ϕ, z) , where the z -axis is aligned with the symmetry axis of the star. Although relativistic effects will certainly play a role in neutron star physics, we will neglect these for this study, and work in Newtonian gravity. We also ignore the elastic crust and any non-hadronic matter that may form an inner core, and assume that the neutron star is a multifluid system, with a neutral fluid of neutrons and a charged fluid of protons and electrons.

Our multifluid model should be applicable for the bulk of a neutron star’s interior during much, but not all, of its life. A neutron star is born hot, with its charged and neutral components strongly coupled through various dissipative mechanisms; at this stage it behaves as a *single*, non-barotropic, fluid. When the star cools below a critical temperature T_c however, the core neutrons begin to condense into a superfluid state¹. The recent observations of the cooling of the Cassiopeia A NS indicate that $T_c \sim (5 - 9) \times 10^8$ K; a NS core should start to drop below this temperature ~ 100 years after birth (Page et al. 2011; Shternin et al. 2011). For this reason, even young pulsars are likely to have substantial multifluid regions — i.e., regions where the neutrons are superfluid. Models of magnetar temperature profiles (Kaminker et al. 2006) indicate they are cool enough to have multifluid regions too. For this preliminary study into stratified NSs we model the *entire* star as multifluid; this is obviously a simplification, and more detailed modelling should account for the layered structure (including single-fluid regions) expected in real NSs.

Now, since electrons have a much smaller mass than either of the other components, we take the standard approach of neglecting their inertia. Our final model is then a two-fluid system, with a proton fluid (whose variables are denoted with a subscript roman index p) and a neutron fluid (with index n). Neutrons and protons are assumed to be of equal mass $m_n = m_p \equiv m$. Next, we denote the particle chemical potentials by μ_n and μ_p , then define $\tilde{\mu}_n \equiv \mu_n/m$ and $\tilde{\mu}_p \equiv (\mu_p + \mu_e)/m$; note that we use $\tilde{\mu}_p$ to denote the chemical potential of the whole charged component, as it also contains a contribution from the electrons μ_e .

In normal MHD, only the protons are coupled to the magnetic field, but for a superfluid/superconducting system there is generally a magnetic force acting on the neutrons as well (Mendell 1991; Glampedakis, Andersson & Samuelsson 2011). In this work however, we only consider the case without entrainment, for which the neutron superfluid is decoupled from the magnetic field in the superconducting case too. This issue is discussed in more detail in Glampedakis, Andersson & Lander

¹ Neutron superfluidity in the inner crust is likely to occur at a higher temperature — above 10^9 K — due to its singlet pairing type (as opposed to the triplet type in the core), making this part of the star a multifluid system too.

(2011). Given these assumptions, we may now state the separate Euler equations which govern the two fluids:

$$\nabla \left(\tilde{\mu}_n + \Phi - \frac{\varpi^2 \Omega_n^2}{2} \right) = 0, \quad (1)$$

$$\nabla \left(\tilde{\mu}_p + \Phi - \frac{\varpi^2 \Omega_p^2}{2} \right) = \frac{\mathbf{F}_{\text{mag}}}{\rho_p}, \quad (2)$$

where \mathbf{F}_{mag} denotes the magnetic force; the form of this force will be the only difference between the normal-MHD and superconducting cases to our order of working. As usual, Φ denotes the gravitational potential, ρ is density and Ω denotes rotation rate (with indices for individual fluid species). We will only consider the case where there is no entrainment and the two fluids corotate, i.e. $\Omega_n = \Omega_p \equiv \Omega$. Since we are only studying stationary configurations, the equations do not contain mutual friction terms.

As in the single-fluid case we have Poisson's equation for the gravitational potential, from which we see that the behaviour of the two fluids is linked despite the neutrons being a superfluid:

$$\nabla^2 \Phi = 4\pi G \rho = 4\pi G(\rho_n + \rho_p). \quad (3)$$

Let us multiply equation (1) by ρ_n , equation (2) by ρ_p , and add them:

$$\rho_n \nabla \tilde{\mu}_n + \rho_p \nabla \tilde{\mu}_p + \rho \nabla \Phi - \rho \nabla \left(\frac{\varpi^2 \Omega^2}{2} \right) = \mathbf{F}_{\text{mag}}. \quad (4)$$

Now since $\rho_n \nabla \tilde{\mu}_n + \rho_p \nabla \tilde{\mu}_p = \nabla P$ (the gradient of the total fluid pressure), this allows us to recover the familiar 'single-fluid' Euler equation:

$$\frac{\nabla P}{\rho} + \nabla \Phi - \nabla \left(\frac{\varpi^2 \Omega^2}{2} \right) = \frac{\mathbf{F}_{\text{mag}}}{\rho}, \quad (5)$$

except that in this two-fluid case one will typically have stratification, and hence can no longer replace the pressure term with an enthalpy gradient. Instead, it is more useful to work with the proton-fluid Euler and a 'difference-Euler', given by (2) minus (1):

$$\nabla (\tilde{\mu}_p - \tilde{\mu}_n) = \frac{\mathbf{F}_{\text{mag}}}{\rho_p}. \quad (6)$$

Taking the curl of this equation, we see that (as in the single-fluid case) there exists a scalar M such that

$$\frac{\mathbf{F}_{\text{mag}}}{\rho_p} = \nabla M. \quad (7)$$

The magnetic force — whether the normal MHD 'Lorentz force' or the flux-tube tension force of a type-II superconductor (see section 3) — therefore depends on a scalar function M and the proton-fluid density ρ_p , as opposed to the single-fluid case where the dependence is on the total mass density: $\mathbf{F}_{\text{mag}}/\rho = \nabla M$. In deriving the equations that govern the behaviour of the magnetic field in the two-fluid case, the only differences from the single-fluid case will be in this density factor; the final magnetic equations will be the same but with ρ replaced by ρ_p .

For our numerical scheme we need to work with the equilibrium equations in integral form; in this section we discuss those equations which hold for all magnetic-field configurations. Firstly, we always have the same form of Poisson's equation for the gravitational potential:

$$\Phi(\mathbf{r}) = -G \int \frac{\rho_n(\mathbf{r}') + \rho_p(\mathbf{r}')}{|\mathbf{r} - \mathbf{r}'|} d\mathbf{r}'. \quad (8)$$

We also have first-integral forms of the proton-fluid Euler equation (2):

$$\tilde{\mu}_p + \Phi - \frac{\varpi^2 \Omega^2}{2} = M + C_p \quad (9)$$

and the difference-Euler (6):

$$\tilde{\mu}_p - \tilde{\mu}_n = M + C_d, \quad (10)$$

where C_p and C_d are the integration constants for the proton and difference-Euler equations, respectively. Finally, for the equation of state we choose an energy functional \mathcal{E} given by

$$\mathcal{E} = k_n \rho_n^{\gamma_n} + k_p \rho_p^{\gamma_p}, \quad (11)$$

a two-fluid analogue of a polytropic model (Prix, Comer & Andersson 2002; Passamonti, Haskell & Andersson 2009). This could also be written in terms of the polytropic indices $N_x = 1/(\gamma_x - 1)$, $x = \{n, p\}$. Note that (11) can be generalised to include cross-terms, corresponding to symmetry energy and entrainment. The chemical potentials are then defined from the energy functional by

$$\tilde{\mu}_x \equiv \left. \frac{\partial \mathcal{E}}{\partial \rho_x} \right|_{\rho_y}, \quad (12)$$

where the index x represents one particle species (neutrons or protons) and the y index represents the other. The other equations of the system depend on the details of the magnetic-field configuration; we discuss these next.

2.2 Normal MHD

The simplest case is when the charged component of the stellar matter is governed by normal MHD. The magnetic force \mathbf{F}_{mag} is then the familiar Lorentz force, given by

$$\mathcal{L} = \mathbf{j} \times \mathbf{B} = \frac{1}{4\pi}(\nabla \times \mathbf{B}) \times \mathbf{B}, \quad (13)$$

where \mathbf{B} is the magnetic field and \mathbf{j} the current. Most studies of NS equilibria have used the normal-MHD equations and have additionally adopted a single-fluid model, where the charged component is the entire fluid — this ansatz has been used by innumerable authors. Recent examples include Tomimura & Eriguchi (2005); Kiuchi & Yoshida (2008); Haskell et al. (2008); Lander & Jones (2009) and Cioffi, Ferrari & Gualtieri (2010), but there are decades of earlier work on single-fluid models — see, e.g., Ferraro (1954) and Roxburgh (1966).

An obvious way to progress is to work with a two-fluid model, but still in normal MHD: the protons are a normal fluid and the neutrons superfluid. This is not just a stepping stone towards the superfluid/superconducting model of Baym, Pethick & Pines (1969) — it already allows us to study the role of stratification in magnetised stars. Furthermore, the interior magnetic field strength in magnetars may well exceed the second critical field $H_{c2} \sim 10^{16}$ G at which superconductivity is destroyed; in this case magnetar matter could indeed be predominantly normal protons and superfluid neutrons (Glampedakis, Andersson & Lander 2011).

Since only the proton fluid is magnetised, the derivations for all equations with magnetic terms proceed in the same manner as the single-fluid case, with factors of ρ replaced by ρ_p ; otherwise they are identical. For this reason we do not give the details here, but the essentially identical single-fluid derivation may be found in various papers (see, e.g., Lander & Jones (2009)). The non-magnetic equations of the system are those discussed in the previous subsection.

In the mixed-field (or purely poloidal field) case we have a Poisson equation for the ϕ -component of the magnetic vector potential too, allowing for the magnetic field to extend outside the star:

$$A_\phi(\mathbf{r}) \sin \phi = \frac{1}{4\pi} \int \frac{\frac{1}{\varpi} f(\tilde{u}) f'(\tilde{u}) + 4\pi \tilde{\omega} M'(\tilde{u}) \rho_p(\tilde{\mathbf{r}})}{|\mathbf{r} - \tilde{\mathbf{r}}|} \sin \tilde{\phi} d\tilde{\mathbf{r}}, \quad (14)$$

where u is a streamfunction; see the next section. In this equation f and M are functions of u , tildes denote dummy variables and primes denote derivatives. In addition, u and A_ϕ are related through $u = \varpi A_\phi$, so the integral in equation (14) may be rewritten in terms of A_ϕ . As mentioned earlier, this integral equation for A_ϕ is identical to the single-fluid version except with a ρ term in the integrand replaced by ρ_p .

The magnetic functions $M(u)$ and $f(u)$ appear to be arbitrary, but in practice we have found only one acceptable functional form for each; this was also the case in our earlier study of single-fluid models (Lander & Jones 2009). In the mixed-field case, we use the following form of M :

$$M_{mix} = \kappa u = \kappa \varpi A_\phi \quad (15)$$

where κ is a constant governing the strength of the Lorentz force. We find that choosing $M(u)$ as a lower or higher power of u results in the code, through equation (14), iterating to an unmagnetised equilibrium solution — and hence only the above choice of M_{mix} is acceptable in our work.

The other magnetic function f in the integral equation for A_ϕ relates to the toroidal component of the field and is defined to be non-zero only within the largest interior closed field line, so there is no exterior toroidal field (and hence no exterior current):

$$f(u) = a(u - u_{\text{max}})^{1.1} H(u - u_{\text{max}}), \quad (16)$$

where u_{max} is the maximum value attained by u within the star and H is the Heaviside step function. The strength of the toroidal component is adjusted by varying the constant a . Other choices of the exponent than 1.1 are possible; we choose this value as it gives a relatively strong toroidal-field component. Choosing a value of unity or less for the exponent gives undesirable behaviour in $f'(u)$, however (Lander & Jones 2009). Finally, whilst adjusting the exponent in (16) allows for configurations with very modest differences, we do not know of any genuinely different functional form of f which is still dependent on u and restricts the toroidal component to the stellar interior.

In the toroidal-field case there is no separate integral equation for the magnetic field. M has a different functional form in the pure-toroidal field case M_{tor} from that in the mixed/pure-poloidal field case M_{mix} . As with other quantities, the two-fluid form of M_{tor} may be found from the single fluid version by replacing ρ with ρ_p :

$$M_{tor} = -\frac{1}{4\pi} \int_0^{\rho_p \varpi^2} \frac{h(\zeta)}{\zeta} \frac{dh}{d\zeta} d\zeta, \quad (17)$$

where h is a function of $\rho_p \varpi^2$, related to the magnetic field by

$$B_\phi = \frac{h(\rho_p \varpi^2)}{\varpi}. \quad (18)$$

We choose $h(\rho_p \varpi^2) = \lambda \rho_p \varpi^2$, where λ is a constant governing the strength of the toroidal field. Once again, all other functional forms appear to result in either divergent magnetic quantities or our numerical scheme iterating to an unmagnetised solution (Lander & Jones 2009).

Note that the difference-Euler (6) for an unmagnetised star shows that the two fluids are in chemical equilibrium. In the magnetic case there is an extra \mathbf{F}_{mag} term — this could be interpreted as a statement that the star is out of chemical equilibrium (Glampedakis, Andersson & Lander 2011). Alternatively, one could adjust the notion of what is meant by ‘chemical equilibrium’. Since the energy functional \mathcal{E} gains an extra contribution from the presence of a magnetic field (Glampedakis, Andersson & Samuelsson 2011), the chemical potentials — defined through (12) — also change accordingly. One could then see equation (6) as quantifying the difference between magnetised and unmagnetised chemical equilibria.

3 MAGNETIC FORCES IN TYPE-II SUPERCONDUCTIVITY

In a typical NS the protons are likely to form a type-II superconductor, where the field penetrates the star through thin fluxtubes (Baym, Pethick & Pines 1969). This results in a magnetic force dependent on the averaged magnetic field \mathbf{B} but also on the first critical field H_{c1} . The result is a fluxtube tension force (Easson & Pethick 1977; Mendell 1991; Glampedakis, Andersson & Samuelsson 2011), quite different from the Lorentz force (13).

The aim of this section is not to give a complete description of the equations governing a star with type-II superconducting protons, but instead to explore how many of the steps from the normal-fluid Grad-Shafranov derivation (see, e.g., Lander & Jones (2009)) also hold in this case. We derive a general ‘interim’ expression for the magnetic field, analogous to the normal-MHD case, at which point one has to specialise to either purely toroidal fields or mixed fields (with purely poloidal fields as a particular limiting case). A key result for mixed fields from the normal-MHD case no longer holds in the superconducting case, and we defer a detailed study of this to a later paper. Instead we concentrate on purely toroidal magnetic fields, where the derivation is more straightforward.

3.1 General form

In Glampedakis, Andersson & Samuelsson (2011), a full derivation of the equations governing a type-II superconducting neutron star is presented. For our purposes, however, only a reduced and simplified set are needed. We consider the case where there is no magnetic force on the neutrons, and neglect small terms like the ‘London field’. Given this, our equations reduce to those of section 2.1, by setting \mathbf{F}_{mag} to be the superconducting magnetic force $\mathfrak{F}_{\text{mag}}$. Before discussing this force, we have one useful result from normal MHD which still holds in this case. Using the fact that $\nabla \cdot \mathbf{B} = 0$ together with the assumption of axisymmetry allows us to write \mathbf{B} in terms of a streamfunction u (Lander & Jones 2009):

$$\mathbf{B} \equiv \mathbf{B}_{\text{pol}} + \mathbf{B}_{\text{tor}} = \frac{1}{\varpi} \nabla u \times \mathbf{e}_\phi + B_\phi \mathbf{e}_\phi. \quad (19)$$

As in normal MHD then, we have $\mathbf{B} \cdot \nabla u = 0$. At this point we turn to equation (153) from Glampedakis, Andersson & Samuelsson (2011) for the explicit form of $\mathfrak{F}_{\text{mag}}$:

$$\mathfrak{F}_{\text{mag}} = \frac{1}{4\pi} \left[(\mathbf{B} \cdot \nabla)(H_{c1} \hat{\mathbf{B}}) - B \nabla H_{c1} \right] - \frac{\rho_p}{4\pi} \nabla \left(B \frac{\partial H_{c1}}{\partial \rho_p} \right), \quad (20)$$

where $\hat{\mathbf{B}}$ is a magnetic unit vector and B is the (position-dependent) magnitude of the field, so that $\mathbf{B} = B \hat{\mathbf{B}}$. From the calculation in appendix A2 of Glampedakis, Andersson & Samuelsson (2011), the first critical field $H_{c1} = h_c \rho_p / \varepsilon_\star$ to a good approximation, where ε_\star is entrainment and h_c a constant parameter. Since we are assuming that there is no neutron-fluid magnetic force, and hence no entrainment, we have $\varepsilon_\star = 1$. The magnetic force then becomes

$$\mathfrak{F}_{\text{mag}} = \frac{h_c}{4\pi} \left[(\mathbf{B} \cdot \nabla)(\rho_p \hat{\mathbf{B}}) - \nabla(B \rho_p) \right]. \quad (21)$$

Now by using a vector identity to rewrite the first term on the RHS and rearranging the result we arrive at:

$$-\frac{4\pi}{h_c} \mathfrak{F}_{\text{mag}} = \rho_p \nabla B + \mathbf{B} \times \left(\rho_p \nabla \times \hat{\mathbf{B}} + \nabla \rho_p \times \hat{\mathbf{B}} \right). \quad (22)$$

Next we want to rewrite the bracketed term on the RHS of equation (22). Let us start by defining a ‘unit current’ $\hat{\mathbf{j}} \equiv \nabla \times \hat{\mathbf{B}}$; as in the single-fluid case it may be shown that

$$\hat{\mathbf{j}} = \frac{1}{\varpi} \nabla(\varpi \hat{B}_\phi) \times \mathbf{e}_\phi + \hat{\mathbf{j}}_\phi \mathbf{e}_\phi. \quad (23)$$

We then decompose both of the bracketed terms from (22) into poloidal and toroidal components. The resultant expression may then be rearranged to show that

$$\rho_p \nabla \times \hat{\mathbf{B}} + \nabla \rho_p \times \hat{\mathbf{B}} = \frac{1}{\varpi} \nabla(\rho_p \varpi \hat{B}_\phi) \times \mathbf{e}_\phi + \left(\rho_p \hat{j}_\phi - \frac{\nabla \rho_p \cdot \nabla u}{\varpi B} \right) \mathbf{e}_\phi \quad (24)$$

The magnetic force becomes

$$-\frac{4\pi}{h_c} \mathfrak{F}_{\text{mag}} = \rho_p \nabla B + \frac{1}{\varpi} \mathbf{B} \times \left(\nabla(\rho_p \varpi \hat{B}_\phi) \times \mathbf{e}_\phi \right) + \left(\rho_p \hat{j}_\phi - \frac{\nabla \rho_p \cdot \nabla u}{\varpi B} \right) \mathbf{B} \times \mathbf{e}_\phi. \quad (25)$$

Again, it is useful to rearrange some terms in this expression. The second term on the RHS of (25) may be rewritten as:

$$\frac{1}{\varpi} \mathbf{B} \times \left(\nabla(\rho_p \varpi \hat{B}_\phi) \times \mathbf{e}_\phi \right) = \frac{1}{\varpi^2} \nabla u \times \nabla(\rho_p \varpi \hat{B}_\phi) + \frac{B_\phi}{\varpi} \nabla(\rho_p \varpi \hat{B}_\phi), \quad (26)$$

using standard vector identities. To simplify the third term on the RHS of (25) we use

$$\mathbf{B} \times \mathbf{e}_\phi = \mathbf{B}_{\text{pol}} \times \mathbf{e}_\phi = -\frac{\nabla u}{\varpi}. \quad (27)$$

Now, putting these two results into the expression for the magnetic force (25) we find that:

$$-\frac{4\pi}{h_c} \mathfrak{F}_{\text{mag}} = \rho_p \nabla B + \frac{1}{\varpi^2} \nabla u \times \nabla(\rho_p \varpi \hat{B}_\phi) + \frac{B_\phi}{\varpi} \nabla(\rho_p \varpi \hat{B}_\phi) + \left(\frac{\nabla \rho_p \cdot \nabla u}{\varpi B} - \rho_p \hat{j}_\phi \right) \frac{\nabla u}{\varpi}. \quad (28)$$

By axisymmetry, the toroidal component of $\mathfrak{F}_{\text{mag}}$ must be zero. Now, all of the terms in the above expression are gradients of scalars (and hence poloidal), except the cross product. This term is purely toroidal and hence must be zero:

$$\frac{1}{\varpi^2} \nabla u \times \nabla(\rho_p \varpi \hat{B}_\phi) = 0. \quad (29)$$

Hence we can remove this term from the magnetic force to arrive at a somewhat simplified result, in terms of the gradients of various scalar functions:

$$-\frac{4\pi}{h_c} \mathfrak{F}_{\text{mag}} = -\frac{4\pi}{h_c} \rho_p \nabla M = \rho_p \nabla B + \frac{B_\phi}{\varpi} \nabla(\rho_p \varpi \hat{B}_\phi) + \left(\frac{\nabla \rho_p \cdot \nabla u}{\varpi B} - \rho_p \hat{j}_\phi \right) \frac{\nabla u}{\varpi}, \quad (30)$$

where M is defined by equation (7), as before. For comparison, the equivalent form for the magnetic force in the normal-MHD derivation (see, e.g., the appendix of Lander & Jones (2009)) is:

$$-4\pi \rho \nabla M = \frac{B_\phi}{\varpi} \nabla(\varpi B_\phi) - 4\pi j_\phi \frac{\nabla u}{\varpi} \quad (31)$$

where $j_\phi = \frac{1}{4\pi} [\nabla \times \mathbf{B}]_\phi$. We see that in the superconducting case there are extra terms with ∇B and $\nabla \rho_p$ factors.

The above derivation is similar in approach to that for the Grad-Shafranov equation of barotropic normal MHD (Lander & Jones 2009), up until the result (30). One remaining step from the normal-MHD derivation cannot, however, be generalised straightforwardly for superconducting matter: we no longer have $\mathbf{B} \cdot \nabla M = 0$ and so in general $M \neq M(u)$. This prevents us from continuing the derivation for poloidal/mixed fields in the normal-MHD manner. Rather than discussing this issue in more detail now, we stop at the interim general result (30) and only consider the simplest specific case, where the magnetic field is purely toroidal. We intend to return to the cases of purely poloidal and mixed poloidal-toroidal fields in future work.

3.2 Purely toroidal fields

For purely toroidal fields, let us return to equation (30). In this case we have $\nabla u = 0$ and the expression for the magnetic force reduces to

$$\mathfrak{F}_{\text{mag}} = \rho_p \nabla M = -\frac{h_c}{4\pi} \frac{1}{\varpi} \nabla(\varpi \rho_p B_\phi), \quad (32)$$

where we have also used $\hat{B}_\phi = 1$. Again, we recall the normal-MHD result (Lander & Jones 2009) for comparison:

$$\mathcal{L} = \rho \nabla M = -\frac{B_\phi}{4\pi \varpi} \nabla(\varpi B_\phi). \quad (33)$$

Now, dividing equation (32) by ρ_p and taking the curl of it yields

$$0 = \nabla \left(\frac{1}{\varpi \rho_p} \right) \times \nabla(\varpi \rho_p B_\phi) = -\frac{1}{\varpi^2 \rho_p^2} \nabla(\varpi \rho_p) \times \nabla(\varpi \rho_p B_\phi). \quad (34)$$

Wherever the magnetic field is non-zero $\varpi \rho_p \neq 0$ too, since this is the geometry of a toroidal field, so we have

$$0 = \nabla(\varpi \rho_p) \times \nabla(\varpi \rho_p B_\phi) \quad (35)$$

and hence the two arguments of the gradient operators are related by some function η :

$$\eta(\varpi \rho_p) = \varpi \rho_p B_\phi. \quad (36)$$

Putting this into (32) and defining $\zeta \equiv \varpi \rho_p$ we get

$$\nabla M = -\frac{h_c}{4\pi} \frac{1}{\zeta} \nabla \eta(\zeta) = -\frac{h_c}{4\pi} \frac{1}{\zeta} \frac{d\eta}{d\zeta} \nabla \zeta \quad (37)$$

where the corresponding magnetic field is

$$\mathbf{B} = B_\phi \mathbf{e}_\phi = \frac{\eta(\zeta)}{\zeta} \mathbf{e}_\phi. \quad (38)$$

The first integral of (37) gives our final result, which may be used in the code:

$$M = -\frac{h_c}{4\pi} \int_0^{\varpi\rho_p} \frac{1}{\zeta} \frac{d\eta}{d\zeta} d\zeta. \quad (39)$$

Not all functional forms of $\eta(\zeta)$ are acceptable choices — for example, taking η to be a linear function of ζ leads to a magnetic force which diverges on the polar axis. In this paper we will work with two other choices of η . The first (which we will refer to as ‘ ζ^2 -superconductivity’ for brevity) is

$$\eta = \eta_0 \zeta^2 \quad (40)$$

with η_0 a constant, which may be varied to adjust the magnetic field strength. With this we have

$$M = -\frac{h_c \eta_0}{2\pi} \varpi \rho_p \quad \text{and} \quad B_\phi = \eta_0 \varpi \rho_p. \quad (41)$$

This form of B_ϕ is the same as that in our normal-MHD toroidal-field case. Note that ζ^2 -superconductivity is the two-fluid equivalent of the case considered by Akgün & Wasserman (2008). The second functional form we will work with (hereafter ‘ ζ^3 -superconductivity’) is

$$\eta = \eta_0 \zeta^3. \quad (42)$$

The magnetic force scalar and magnetic field in this case are given by

$$M = -\frac{3h_c \eta_0}{8\pi} \varpi^2 \rho_p^2 \quad \text{and} \quad B_\phi = \eta_0 \varpi^2 \rho_p^2. \quad (43)$$

At this stage, our motivation for choosing these two functional forms is their simplicity. Later, we will find that the resulting equilibria in the two cases are very similar, suggesting that our results may be quite generic.

4 NUMERICS

4.1 Overview of code

The code we use iteratively solves the equilibrium equations for our neutron star model, and being non-linear is not restricted to the perturbative regime of slow rotation and weak magnetic fields. Our numerical scheme is based on the Hachisu self-consistent field (SCF) method (Hachisu 1986), a more robust extension of an earlier SCF method by Ostriker & Mark (1968). A version of the Hachisu SCF method for magnetised stars was presented by Tomimura & Eriguchi (2005). Since our scheme is a fairly straightforward extension of these previous ones, we content ourselves with a summary here and focus on the differences between them; we refer the reader to Hachisu (1986) and Tomimura & Eriguchi (2005) for more details.

To find equilibrium models, the user must specify a number of stellar parameters at the outset. The major ones are related to:

1. the EOS — through the polytropic indices N_n and N_p (related to the compressibility of each fluid);
2. the shape of the star (related to the rotation rate) — specified through the ratio of polar to equatorial radii r_{pole}/r_{eq} , and the ratio of the neutron-fluid equatorial surface to the proton-fluid equatorial surface r_{eq}^n/r_{eq}^p ;
3. the magnetic field — through κ and a for normal-MHD mixed fields (or poloidal fields), λ for normal-MHD toroidal fields, and η_0 for toroidal fields in a superconductor. See sections 2.2 and 3.2 for more details.

We nondimensionalise all quantities within the code using the requisite combination of r_{eq} , G and ρ_{\max} and use a hat to denote these dimensionless quantities. As a consequence we have $\hat{r}_{eq} = \hat{\rho}_{\max} = 1$. When calculating integrals we first decompose the integrands into radial pieces and Legendre polynomials (note that there is no azimuthal piece, since we work in axisymmetry). The contributions over all relevant grid points are then summed up appropriately. We include angular contributions up to degree $l = 32$ in the Legendre polynomials, thus allowing for magnetic configurations of high multipolar structure, in contrast with the dipolar models of Glampedakis, Andersson & Lander (2011).

4.2 Finding integration constants and the rotation rate

To find the stellar rotation rate and integration constants of the Euler equations we have to evaluate these equations at suitable boundaries. Typically the two fluid surfaces do not coincide, and there are different procedures to calculate these constants depending on whether the proton or neutron fluid is outermost. However, we know *a posteriori* that all our configurations have the proton fluid either outermost or coincident with the neutron surface, so we only consider that case here.

For this, we work with the proton-fluid Euler and the difference Euler and aim to find C_p , C_d and Ω ; recall that we assume that both fluids have the same rotation rate, $\Omega_n = \Omega_p = \Omega$. In this section we define each fluid surface by the vanishing of

its corresponding chemical potential $\tilde{\mu}_x = 0$; this approach was also used by Yoshida & Eriguchi (2004) and avoids numerical difficulties associated with dealing with the true fluid surfaces — those given by $\rho_x = 0$. In general the two definitions do not agree, due to coupling between the different fluids (Prix, Novak & Comer 2005), and in practice one would expect an interior phase transition rather than a sharp fluid surface. Despite these issues, working with the $\tilde{\mu}_x = 0$ surfaces is sufficient for our simplified model of a two-fluid NS. In section 5.2 we describe how to check the surfaces of the redimensionalised, physical, star.

This subsection requires the user-specified stellar axis ratio r_{pole}/r_{eq} (which is the same as the proton-fluid axis ratio r_{pole}^p/r_{eq}^p). In our dimensionless units the axis ratio is equal to the dimensionless polar radius of the proton fluid \hat{r}_{pole}^p . The neutron-surface equatorial radius $\hat{r}_{eq}^n = r_{eq}^n/r_{eq}^p$ is also used here. We begin by evaluating (9) at the equatorial stellar surface $\hat{r}_{eq} = 1$:

$$\hat{\mu}_p(1) = 0 = \hat{C}_p + \hat{M}(1) + \frac{\hat{\Omega}^2}{2} - \hat{\Phi}(1). \quad (44)$$

and at the polar stellar surface $\hat{r}_{pole}(=\hat{r}_{pole}^p)$:

$$\hat{\mu}_p(\hat{r}_{pole}) = 0 = \hat{C}_p + \hat{M}(\hat{r}_p) - \hat{\Phi}(\hat{r}_p). \quad (45)$$

We may combine the above expressions to find Ω and C_p :

$$\hat{\Omega}^2 = 2\left(\hat{M}(\hat{r}_{pole}) - \hat{M}(1) - \hat{\Phi}(\hat{r}_{pole}) + \hat{\Phi}(1)\right) \quad (46)$$

$$\hat{C}_p = \hat{\Phi}(1) - \frac{\hat{\Omega}^2}{2} - \hat{M}(1). \quad (47)$$

Note that we have $M \propto \rho_p$ for a toroidal field (in both normal and superconducting matter) and so is zero at the stellar surface; in this case the expressions for Ω and C_p have no explicit dependence on the magnetic force. Now evaluating the difference Euler at the *neutron-fluid surface*, rather than the stellar surface, we determine C_d :

$$\hat{C}_d = \hat{\mu}_p(\hat{r}_{eq}^n) - \hat{M}(\hat{r}_{eq}^n). \quad (48)$$

4.3 Iterative step

We recall that the chemical potentials are defined from the energy functional \mathcal{E} by

$$\tilde{\mu}_x \equiv \left. \frac{\partial \mathcal{E}}{\partial \rho_x} \right|_{\rho_y}. \quad (49)$$

For our particular functional (11), the resulting expressions for the chemical potentials may be rearranged to give

$$\rho_n = \left(\frac{\tilde{\mu}_n}{k_n \gamma_n} \right)^{N_n}, \quad \rho_p = \left(\frac{\tilde{\mu}_p}{k_p \gamma_p} \right)^{N_p}. \quad (50)$$

Evaluating these at the centre of the star we obtain relations between the maximum values of the chemical potential and density for each fluid. In dimensionless form these may be rearranged to show that

$$\hat{k}_p \gamma_p = \hat{\mu}_p^{\max} x_p(0)^{-1/N_p}, \quad \hat{k}_n \gamma_n = \hat{\mu}_n^{\max} (1 - x_p(0))^{-1/N_n}, \quad (51)$$

where $x_p(0)$ is the central proton fraction, using the fact that $\hat{\rho}_p = \rho_p/\rho = x_p$ and similarly $\hat{\rho}_n = (1 - x_p)$. Comparing these relations with those in (50) we obtain expressions which will allow us to iterate for new density distributions within our numerical scheme:

$$\hat{\rho}_p = x_p(0) \left(\frac{\hat{\mu}_p}{\hat{\mu}_p^{\max}} \right)^{N_p}, \quad \hat{\rho}_n = (1 - x_p(0)) \left(\frac{\hat{\mu}_n}{\hat{\mu}_n^{\max}} \right)^{N_n}. \quad (52)$$

4.4 Iterative procedure

We now have all equations needed for the iterative procedure that generates our equilibria. As discussed at the start of this section, the procedure is an extension of the Hachisu SCF method (Hachisu 1986; Tomimura & Eriguchi 2005). To begin the iterative process (step 0), we set the two fluid densities and the magnetic potential to be constant within the star; however, we have found that the final equilibria are independent of the values chosen at this step. Note that for a toroidal field — in normal or superconducting matter — there is no separate iteration for the magnetic field and hence no step 2; instead the behaviour of the field is directly linked to ρ_p . The iterative steps are as follows:

0. For the initial iteration, start with a guess that ρ_n, ρ_p and A_ϕ are all constant;
1. Calculate the gravitational potential Φ from the ρ_n and ρ_p distributions and Poisson's equation (8);
2. Calculate the new magnetic potential component A_ϕ from its value at the previous iteration A_ϕ^{old} , using the magnetic

Poisson equation (14) with A_ϕ^{old} and ρ_p in the integrand;

3. Evaluate the proton-fluid Euler (9) at the equatorial and polar surface, using boundary conditions on $\tilde{\mu}_p$; this gives two equations which fix Ω^2 and then C_p ;
4. We are now able to use the proton-fluid Euler to find $\tilde{\mu}_p$ throughout the star;
5. Evaluate the difference-Euler (10) at the equatorial neutron-fluid surface to find C_d ;
6. Now use the difference-Euler to find $\tilde{\mu}_n$ throughout the star;
7. Calculate the new density distributions from the chemical potentials, using the expressions in (52);
8. Return to step 1 using the new ρ_n, ρ_p and A_ϕ ; repeat procedure until satisfactory convergence is achieved (i.e. until the difference between quantities at consecutive iterative steps is less than some small tolerance).

5 STELLAR PARAMETERS AND SEQUENCES

5.1 Redimensionalising

When looking at sequences of configurations, to study the effect of magnetic fields or rotation, we need to ensure we are always working with the same physical star — the dimensionless quantities produced by the code are not sufficient. Two stars are physically the same if they have the same mass and equation of state: $\mathcal{M}, \gamma_n, \gamma_p, k_n$ and k_p must all be equal for both. Since we specify the (dimensionless) indices γ_n and γ_p at the outset, we only need to fix the physical values of \mathcal{M}, k_n and k_p .

Fixing the stellar mass is straightforward — we choose $\mathcal{M} = 1.4\mathcal{M}_\odot$ (where \mathcal{M}_\odot is one solar mass) — but more care is needed with the polytropic constants. We choose to fix their physical values in the following way: take a spherical star in hydrostatic equilibrium (nonrotating and with no magnetic field), with some fixed γ_n and γ_p and coincident neutron and proton surfaces. Now find the polytropic constants k_n, k_p that give it a radius of 10 km. More specifically, the dimensionless mass and polytropic constants are related to their physical counterparts through:

$$\hat{\mathcal{M}} = \frac{\mathcal{M}}{\rho_{\max} r_{eq}^3}, \quad \hat{k}_x = \frac{k_x}{Gr_{eq}^2 \rho_{\max}^{\gamma_x - 2}}. \quad (53)$$

Having specifying a spherical configuration with some particular γ_x , the code may be used to calculate $\hat{\mathcal{M}}$ and \hat{k}_x . The requirement that $\mathcal{M} = 1.4\mathcal{M}_\odot$ and $r_{eq} = 10$ km for the spherical configuration then fixes the physical value of k_x for the stellar sequence; from this we may find ρ_{\max} and r_{eq} for any star in the sequence, and hence redimensionalise any other quantities (e.g. rotation rates and field strengths). Any rotating, magnetised configuration redimensionalised in this manner will be the same physical star: if you stopped it from rotating and removed its magnetic field, it would return to the same 10 km spherical body.

5.2 Adjusting the position of the fluid surfaces

Our iterative procedure does not automatically adjust the location of the neutron surface, even though it will change with respect to the proton surface when the star is rotating or magnetised. A rotating or magnetised star in which the two fluids coincide at the equator would *not* return to our canonical unmagnetised nonrotating spherical star with coincident fluid surfaces. This means that the physical values of the polytropic constants k_x would be different in the two cases. Instead we have to manually adjust the location of the neutron-fluid equatorial surface so that the values of k_x *do* agree with those of our canonical physical star. In practice the difference between the fluid surfaces is only significant at high rotation rates or magnetic field strengths, and for the purposes of this study a simple root-finder algorithm can be employed to run the code a few times, adjusting the neutron-surface until satisfactory results are achieved.

5.3 Virial test

The scalar virial theorem, which is derived from the (sum) Euler equation, states that a certain combination of energies balances the acceleration of the system. For a single-fluid polytrope:

$$2T + \mathcal{E}_{\text{mag}} + W + 3(\gamma - 1)U = \frac{1}{2} \frac{d^2 I}{dt^2} \quad (54)$$

where $T, \mathcal{E}_{\text{mag}}, W$ and U are, respectively, the kinetic, magnetic, gravitational and internal energies of the system, and I is the moment of inertia. For our ‘separable’ equation of state, where each fluid obeys its own polytropic relation, this relation may be generalised simply:

$$2T + \mathcal{E}_{\text{mag}} + W + 3(\gamma_n - 1)U_n + 3(\gamma_p - 1)U_p = \frac{1}{2} \frac{d^2 I}{dt^2}. \quad (55)$$

Since we seek equilibrium configurations, we can test the accuracy of our code by how close the residual acceleration of the system (i.e. the right-hand side of the previous equation) is to zero. We then form a dimensionless quantity by normalising

this acceleration through division by W :

$$\text{'virial test'} \equiv \text{error} = \frac{|2T + \mathcal{E}_{\text{mag}} + W + 3(\gamma_{\text{n}} - 1)U_{\text{n}} + 3(\gamma_{\text{p}} - 1)U_{\text{p}}|}{|W|}. \quad (56)$$

5.4 Ellipticity

Our numerical scheme involves specifying some axis ratio $r_{\text{pole}}/r_{\text{eq}}$, corresponding to the surface shape of the star. A more informative quantity however is the ellipticity, which measures the deviation of the whole mass distribution from sphericity. Starting from the mass quadrupole moment tensor

$$Q_{jk} = \int \rho x_j x_k \, dV \quad (57)$$

where x_j, x_k are Cartesian coordinates, we define the ellipticity of the star through the components of the quadrupole moment at the equator Q_{xx} and pole Q_{zz} :

$$\epsilon = \frac{Q_{xx} - Q_{zz}}{Q_{xx}}. \quad (58)$$

5.5 Magnetic-field quantities

The conventional definition of the (normal-MHD) magnetic energy is as an integral out to infinite radius:

$$\mathcal{E}_{\text{mag}} = \frac{1}{8\pi} \int_{\text{all space}} B^2 \, dV, \quad (59)$$

which would have to be truncated on our finite numerical grid. One alternative but equivalent form of \mathcal{E}_{mag} is as the integral of $\mathbf{r} \cdot \mathcal{L}$; this may be seen from the relevant part of the virial theorem derivation (Chandrasekhar 1961). Since \mathcal{L} is only non-zero over the star (by virtue of its ρ_{p} factor), we may write the magnetic energy as

$$\mathcal{E}_{\text{mag}} = \int_{\text{star}} \mathbf{r} \cdot \mathcal{L} \, dV. \quad (60)$$

The magnetic energy in the toroidal component of the field is also an integral over the star:

$$\mathcal{E}_{\text{tor}} = \frac{1}{8\pi} \int_{\text{star}} B_{\phi}^2 \, dV, \quad (61)$$

since $B_{\phi} = 0$ outside the star. Finally, it is clear that the poloidal-field contribution to the energy is simply $\mathcal{E}_{\text{mag}} - \mathcal{E}_{\text{tor}}$, so there is no need to use an integral out to infinity for this case either.

When looking at mixed-field configurations, we want some measure of the relative strength of the toroidal and poloidal field components. We do this in two ways: one related to the global contributions of each component and one which looks at their maximum values. For the former, we take the percentage of the magnetic energy stored in the toroidal component $\mathcal{E}_{\text{tor}}/\mathcal{E}_{\text{mag}}$; this is relevant for understanding quantities like the ellipticity, which scale with B^2 . For the latter we compare the maximum value attained by each field component, using the ratio

$$\frac{B_{\text{tor}}^{\text{max}}}{B_{\text{tor}}^{\text{max}} + B_{\text{pol}}^{\text{max}}}. \quad (62)$$

Unlike the more obvious choice of $B_{\text{tor}}^{\text{max}}/B_{\text{pol}}^{\text{max}}$, the ratio (62) varies from zero (no toroidal field) to unity (purely toroidal field), which is perhaps clearer.

Although a number of studies have used the energy ratio $\mathcal{E}_{\text{tor}}/\mathcal{E}_{\text{mag}}$ to assess the stability of a magnetic-field configuration (see, e.g., Braithwaite (2009)), this is a global quantity, whereas the relevant instability is highly localised — around the neutral point for a purely poloidal field (Markey & Tayler 1973). To remove this instability, what is more important is whether the toroidal component is *locally* comparable in strength with the poloidal one (Wright 1973). Since the strength of the poloidal component in the closed-field line region is directly related to its maximum value, we argue that the ratio (62) may be a better indication of the stability of a configuration.

Since we are interested in the effect of a magnetic field on the global properties of neutron stars, we work with a volume-averaged form of the magnetic field \bar{B} rather than a surface value:

$$\bar{B}^2 \equiv \frac{1}{V} \int_{\text{all space}} B^2 \, dV = \frac{8\pi\mathcal{E}_{\text{mag}}}{V}, \quad (63)$$

where V is the star's volume. This volume-averaged value is approximately double the polar surface value B_{pole} for a poloidal field (for a toroidal field the surface value is zero).

For superconducting configurations we have to fix the value of the first critical field strength H_{c1} . This is not a constant,

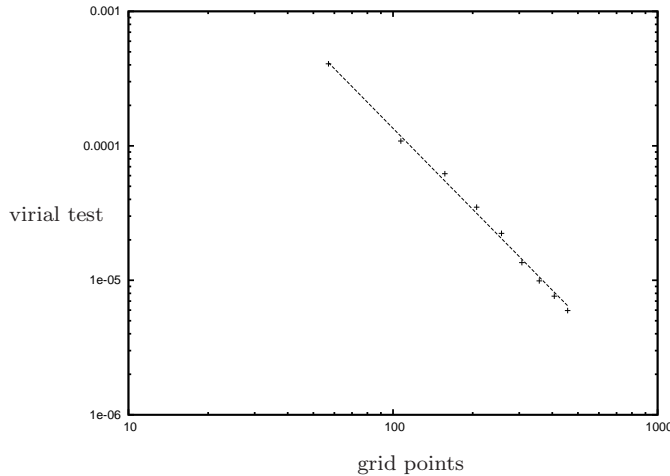


Figure 1. Testing the order of convergence for our code, by plotting the virial test result against the number of grid points. All results are for a rotating magnetised NS model, stratified with $N_n = 1$ and $N_p = 2$, with $\bar{B} = 1.2 \times 10^{17}$ G and $\Omega = 650$ Hz. The line drawn shows the expected result for second-order convergence; it agrees well with the actual points from different resolutions.

Table 1. Comparing with the unmagnetised two-fluid models presented in Prix and Rieutord. The values shown for the polytropic constants and masses are our results, in our dimensionless units, with the discrepancy from those of Prix and Rieutord indicated in brackets.

	γ_n	γ_p	\hat{k}_n	\hat{k}_p	\hat{M}
Model I	2.0	2.0	0.7074 (0.1%)	6.366 (0.1%)	1.273 (0.5%)
Model II	2.5	2.1	0.7060 (0.5%)	9.034 (1.4%)	1.834 (0.7%)
Model III	1.9	1.7	0.6802 (0.7%)	3.466 (0.9%)	1.083 (1.0%)

but is related to ρ_p and hence position-dependent. Unless stated otherwise, we fix the central (i.e. maximum) value of the field to be $H_{c1}(0) = 10^{16}$ G, to fit with the estimate from Glampedakis, Andersson & Samuelsson (2011). This corresponds to a volume-averaged value of $\bar{H}_{c1} \approx 3 \times 10^{15}$ G.

6 RESULTS

Our results are divided into four subsections. We begin by testing the convergence properties of the code and comparing our results with those of previous studies. We then present results for two-fluid stars in normal MHD, focussing on the effect of stratification. In the third subsection we study configurations where the protons form a type-II superconductor, and in the fourth subsection we give approximate relations for the magnetic ellipticity of stars as a function of field strength.

6.1 Tests of the code

Before we present results for our NS models, we test how accurate our code is by using the virial test (56) to determine the relative error in calculating an equilibrium configuration for different numbers of grid points; see figure 1. We see that the error decreases quadratically with resolution, and hence is second-order convergent, as intended.

Next, we compare our results with the three nonrotating and unmagnetised two-fluid models presented in Prix & Rieutord (2002). To do this we need to convert from their dimensionless quantities to ours, using the speed of light $c = 3.00 \times 10^{10}$ cm s $^{-1}$ and nuclear density $\rho_{nuc} = 1.66 \times 10^{14}$ g cm $^{-3}$. Some algebra shows that our dimensionless polytropic constants (denoted by the index *LAG*) and those of Prix & Rieutord (2002) (with index *PR*) are related by

$$\hat{k}_x^{LAG} = \frac{c^2}{Gr_{eq}^2 \rho_{nuc}} \left(\frac{\rho_{max}}{\rho_{nuc}} \right)^{\gamma_x - 2} \hat{k}_x^{PR} = 8.11 \times 10^3 \left(\frac{r_{eq}}{\text{km}} \right)^{-2} \left(\frac{\rho_{max}}{\rho_{nuc}} \right)^{\gamma_x - 2} \hat{k}_x^{PR}. \quad (64)$$

Next we consider the conversion of dimensionless masses:

$$\hat{M}^{LAG} = 12000 \left(\frac{\rho_{max}}{\rho_{nuc}} \right)^{-1} \left(\frac{r_{eq}}{\text{km}} \right)^{-3} \hat{M}^{PR}. \quad (65)$$

Now using these, we can make a direct comparison between our results and those of Prix & Rieutord (2002) — see table 1.

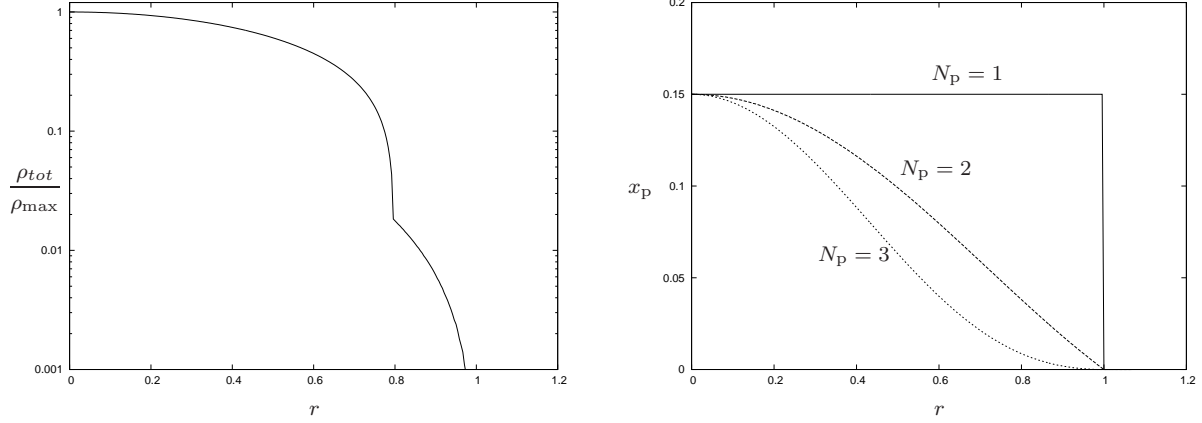


Figure 2. Demonstrating the additional flexibility possible with a two-fluid stellar model. Left: an approximation to the Douchin-Haensel EOS for a fluid core and a solid crust, plotting the total fluid density $\rho_{tot} = \rho_n + \rho_p$ against radius r . In Douchin and Haensel, the core is fairly close to a polytrope with index $N_{core} \approx 0.7$ and the crust is similar to a different polytrope, having $N_{crust} \approx 1.5$, with a crust-core boundary at $\approx 0.03\rho_{max}$ and central proton fraction $x_p(0) = 0.15$. In our model we have $x_p(0) = 0.15$ and $N_{core} \approx N_n = 0.7$, while $N_{crust} \approx N_p = 1.3$. This gives us a density of $\sim 0.02\rho_{max}$ at the crust-core boundary, with a 2 km-thick ‘crust’ for a 10 km radius star. Right: the change in proton fraction x_p against radius. We fix $N_n = 1$ and look at the variation of proton fraction with N_p . In the unstratified case, $N_p = N_n = 1$, the proton fraction is constant within the star.

6.2 Two-fluid equilibrium configurations in normal MHD

Our two-fluid formalism gives us a great deal of flexibility, but for clarity we will present results using just a few canonical values. For unstratified models, we set $N_n = N_p = 1$; whilst when we refer to stratified models we have taken $N_n = 1$ and $N_p = 2$ unless otherwise stated (see the following figure for justification of this choice). In addition, we have fixed the central value of the proton fraction $x_p(0)$ to be equal to 0.15 for all results, although we have found that our results are virtually independent of the value chosen. In many figures, we show stars whose magnetic fields are (probably) unphysically high — of the order of 10^{17} G. This is to emphasise effects which would be less obvious at lower values. We do, however, discuss the scaling of our results to more typical NS field strengths too.

In this section we present results for neutron star models composed of superfluid neutrons and normal-fluid protons, subject to a magnetic field. As discussed above, this situation may apply to an interior region of magnetars, where it is conceivable that the second critical field H_{c2} will be exceeded. Below this critical field the protons will be superconducting, and we cover this case in the following subsection.

In figure 2 we show the additional flexibility possible in two-fluid models. We can model the effect of having a fluid core surrounded by a crust, by allowing the two fluids to terminate at different points, so that there is an outer region with only one of the fluid species — in this case the protons. This is shown in the left-hand plot, where we attempt to fit the equation of state described in Douchin & Haensel (2001) by adjusting parameters in our model accordingly. Two-fluid models also allow us to have stratification and consequently a non-uniform proton fraction, as one would expect in real NSs (Kaminker, Haensel & Yakovlev 2001); see the right-hand plot. Comparing this plot with figure 1 from Glampedakis, Andersson & Lander (2011) showing proton fractions in more sophisticated models, we see that choosing $N_p = 2$ produces a reasonable-looking proton-fraction profile.

Before turning to the effect of a magnetic field on a two-fluid star, we consider the role of rotation on it. This allows us to make contact with models in previous work, as well as giving us some intuition about what to expect from magnetic fields. In figure 3 we show two configurations rotating at their Keplerian frequency. The left-hand star is an unstratified model ($N_n = N_p = 1$) and both fluid surfaces coincide. The interior density contours are different, however, because the central proton fraction $x_p(0) = 0.15$; were it $x_p(0) = 0.5$ then each species would have the same density contours too. The right-hand star is a stratified model and in this case it is the outer fluid, the protons, that determine the star’s breakup velocity — the neutron surface is more rounded, without the characteristic cusped-shape of a fluid at breakup (Prix, Novak & Comer 2005). If we had $N_n > N_p$, the neutron fluid would be outermost; however, we do not consider this case. Instead the protons in our models are always outermost, for rotating configurations but also magnetised ones, as we will see later in this section.

Whilst our formalism is able to deal with stars that are both highly magnetised and rapidly rotating, we will concentrate on non-rotating models from now on. This is because we are chiefly concerned with the effect of stratification on magnetic fields in stars; allowing for the extra effect of rotation obfuscates the picture. This makes our results most directly applicable to magnetars (which rotate very slowly), but the ellipticity formulae presented at the end of this results section are equally applicable to the magnetic distortions in less-magnetised NSs (like pulsars).

We begin by looking at stars with a purely poloidal magnetic field - figure 4. We show contours of the streamfunction u , which are parallel to magnetic field lines, shading the closed-field line region and marking the ‘neutral line’ (where the field

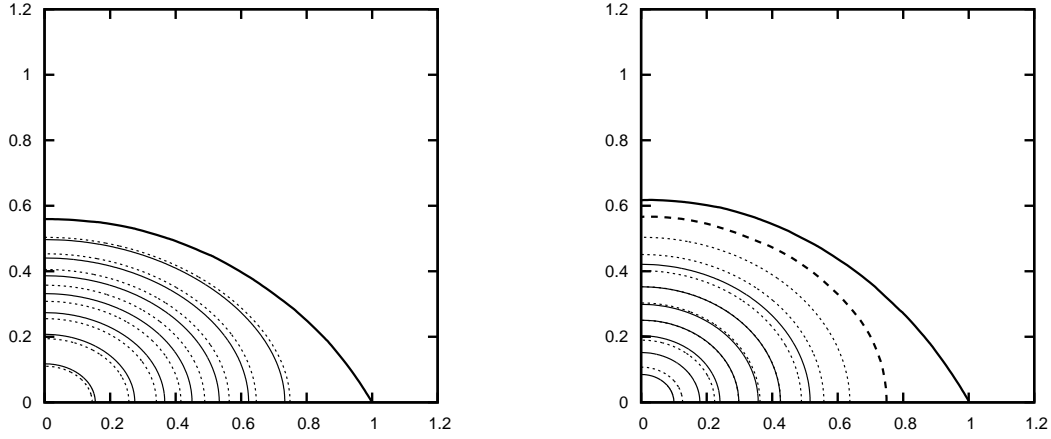


Figure 3. Density contours of two unmagnetised stellar configurations rotating at breakup velocity, left: our canonical unstratified model ($N_n = N_p = 1$), right: our canonical stratified model ($N_n = 1$ and $N_p = 2$). The bold lines show the fluid surfaces — which are coincident for the unstratified star. For the stratified star the neutron fluid is not rotating at breakup velocity, but the proton fluid is.

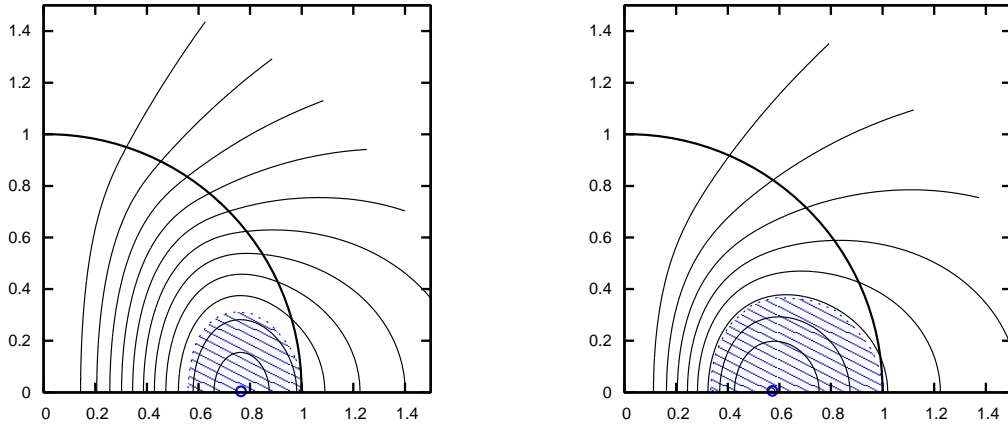


Figure 4. Contours of the streamfunction u for a star with a purely poloidal field, corresponding to magnetic field lines. The thick arc indicates the stellar surface, at a dimensionless radius of unity; the shaded area indicates the closed-field line region, and the small circle on the x -axis shows the location of the neutral line, where the field strength vanishes. Left: no stratification ($N_n = N_p = 1$), right: a stratified model, with $N_n = 1$ and $N_p = 3$. The closed field line region is bigger in the stratified case.

vanishes) with a circle. The field configuration of the unstratified model is very similar to that of a single-fluid polytrope with index $N = 1$ (see, e.g., figure 3 from Lander & Jones (2009)). Stratification has the effect of moving the neutral line inwards and increasing the volume of the closed-field line region. Fixing $N_n = 1$, we find that the greater the value of N_p , the larger the closed-field line region; we have emphasised the effect by taking $N_p = 3$ rather than our canonical choice of $N_p = 2$.

The toroidal-field component of a mixed-field star is defined by a function $f(u)$, which can only be non-zero within the closed-field line region, and by the coefficient a (see equation (16)). Increasing a increases the percentage of magnetic energy stored in the toroidal-field component, and also the maximum value it attains relative to the poloidal component, but it *decreases* the volume of the torus containing the toroidal-field component; see figure 5. This seems to limit the size of the toroidal component, as in the barotropic case (Lander & Jones 2009; Cioffi, Ferrari & Gualtieri 2010). The volume of the torus is increased somewhat for higher values of N_p , however.

In figure 6 we show the variation of magnetic field strength within a typical mixed-field stratified configuration. The field reaches a local maximum in two places — the centre of the star (corresponding to the maximum value of the poloidal component) and near the equatorial surface (the toroidal-component maximum). The toroidal component vanishes at the stellar surface, but the poloidal component extends outside the star (not shown). The configuration shown has 4.7% toroidal energy, around the maximum value possible within our approach. The surface field strength is about 20% of the central value, about 50% of the maximum toroidal field strength and also about 50% of the volume-averaged field strength \bar{B} .

Next we turn to the effect of the magnetic field on the density distribution of the star. We begin with purely poloidal fields, in figure 7. As in the single-fluid barotropic case, these make the star oblate, but virtually all of the distortion is in

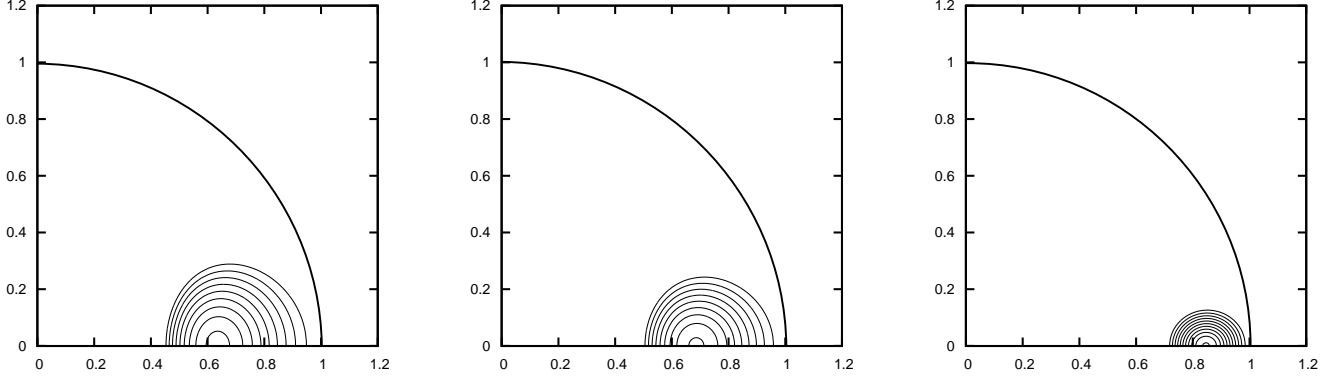


Figure 5. Effect of increasing a , the coefficient of the magnetic function $f(u)$, within a stratified star. Contours of the toroidal field component are shown. As a is increased, from left to right, the percentage of toroidal field increases (1%, 3% and 4.5%), with a corresponding increase in the ratio $B_{\text{tor}}^{\text{max}} / (B_{\text{pol}}^{\text{max}} + B_{\text{tor}}^{\text{max}})$ — from 0.10 to 0.18, and finally 0.34. At the same time, however, the size of the toroidal-field region is decreased.

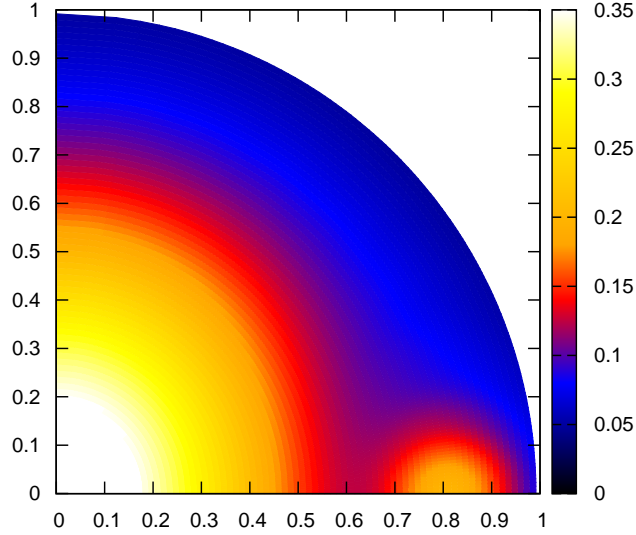


Figure 6. Magnetic field strength within a stratified nonrotating NS with 4.7% toroidal energy. The toroidal field is contained within the small region near the equatorial surface, reaching its maximum at $x \approx 0.8$. The poloidal field pervades the rest of the star, reaching a maximum at the centre. The surface field strength is about 20% of the central value, 50% of the maximum toroidal-component strength and 50% of the average value \bar{B} .

the proton fluid, with the neutron fluid remaining nearly spherical. The two fluid surfaces coincide at the pole, but at the equator the Lorentz force distorts the proton fluid, resulting in a single-fluid region composed only of protons. To make the effect noticeable, we have shown a highly magnetised model, with $\bar{B} \sim 10^{17}$ G. The single-fluid region is analogous to the case of a rotating stratified star with no magnetic field; see figure 3. As mentioned in figure 2 and also by Prix, Novak & Comer (2005), this single-fluid region can be thought of as an approximation to a neutron-star crust.

The unstratified (left) and stratified (right) plots of figure 7 are very similar; the only obvious difference is that when $N_p = 2$ the protons have a larger low density region than the $N_n = 1$ case (this is true in unmagnetised stars too). We have not included density contours for mixed-field stars, as these are very similar to those in figure 7, with the contour lines pushed outwards slightly in the region where the toroidal component is located.

In figure 8 we show density contours of a stratified star with a purely toroidal magnetic field. Again, the neutron fluid is virtually spherical and unaffected by the magnetic field, whilst the proton fluid is highly distorted — into a prolate configuration this time. Note that whilst the innermost proton-density contours are noticeably prolate, the outer ones become virtually spherical; the same effect was seen in the (single-fluid) models of Ostriker & Hartwick (1968), who considered mixed fields but with a dominant toroidal component. Related to this effect, the surfaces of the two fluids are seen to be coincident (or very close to being so). The unstratified case is very similar, just with more evenly-spaced proton-density contours (as

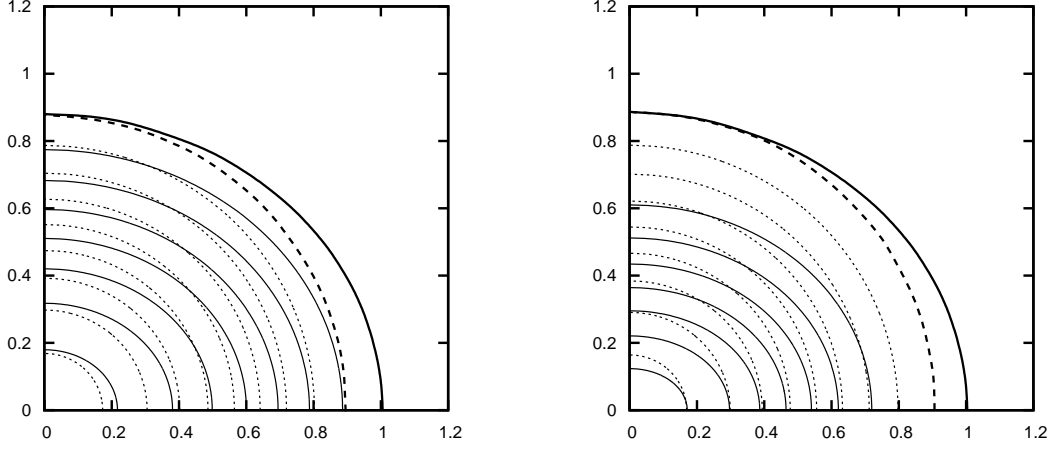


Figure 7. Density contours for proton fluid (solid line) and neutron fluid (dashed) in non-rotating stars distorted by purely poloidal magnetic fields. The bold lines represent the fluid surfaces, which coincide at the pole but not the equator. The proton fluid is seen to be more distorted, due to the magnetic field. The left and right plots show our canonical unstratified and stratified models, respectively.

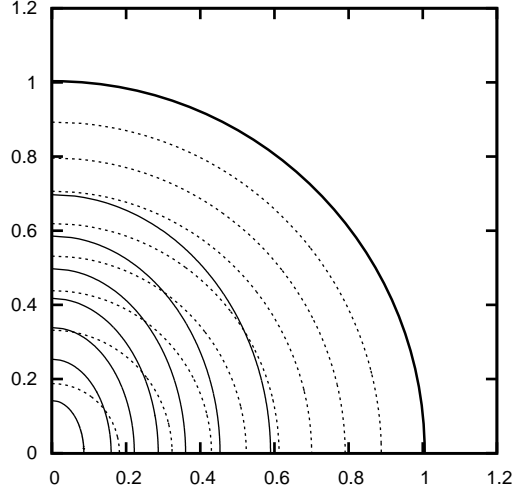


Figure 8. Density contours for proton fluid (solid line) and neutron fluid (dashed) in a non-rotating stratified star with a purely toroidal magnetic field. The bold line represents the two (virtually coincident) fluid surfaces, and hence the stellar surface. Again, the proton fluid is seen to be more distorted, due to the magnetic field.

for the previous figure) — it will be shown in the following subsection, when we compare toroidal fields in normal MHD and superconductivity.

In figure 9 we explore mixed-field configurations with the maximum possible toroidal component (within our models, at least). We use two different measures of the relative strength of the toroidal component: comparing the maximum values of the two field components using the ratio $B_{\text{tor}}^{\text{max}}/(B_{\text{tor}}^{\text{max}} + B_{\text{pol}}^{\text{max}})$ and looking at the contribution of the toroidal component to the total magnetic energy, $\mathcal{E}_{\text{tor}}/\mathcal{E}_{\text{mag}}$. Fixing $N_n = 1$ as usual, we find that for increasing N_p the energy percentage increases, but the relative maximum value of the toroidal component decreases. In all cases the toroidal component is smaller — especially in terms of $\mathcal{E}_{\text{tor}}/\mathcal{E}_{\text{mag}}$. Note that all configurations plotted are close to spherical (with an axis ratio of $r_{\text{pole}}/r_{\text{eq}} = 0.996$). Very highly distorted stars (with consequently strong magnetic fields) can have slightly larger values of $\mathcal{E}_{\text{tor}}/\mathcal{E}_{\text{mag}}$.

Finally in this section, we plot the dependence of ellipticity on magnetic field strength, figure 10. The relation is quadratic, as expected from the single-fluid case, and does not appear to depend on the stratification of the star. We show distortions of a purely poloidal field star, and one with a relatively strong mixed field, 3% toroidal energy. The toroidal component decreases the oblateness of the star, as expected, but we are not able to generate mixed-field configurations where the toroidal component is strong enough to induce a *prolate* distortion. We are only able to produce prolate distortions when the magnetic field is purely toroidal; this case is covered in the next section.

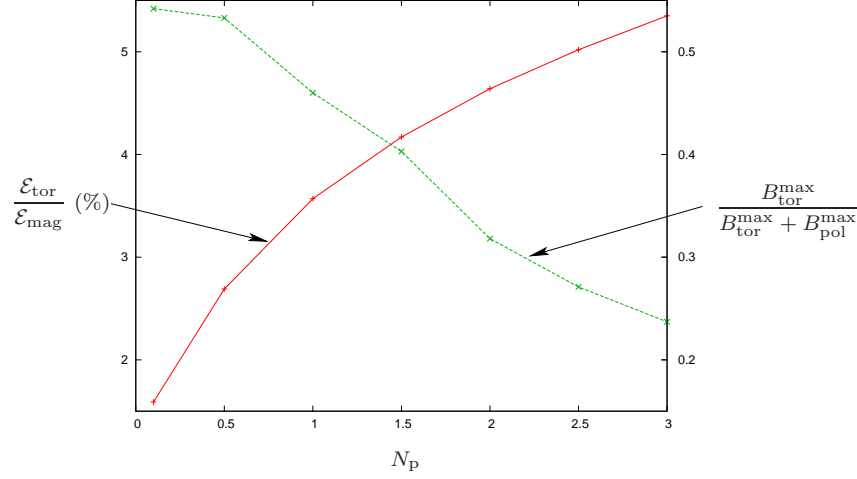


Figure 9. Mixed-field configurations with the maximum possible toroidal component, as a function of N_p . All configurations have $N_n = 1$, are nonrotating and have axis ratios close to unity. The central proton fraction $x_p(0) = 0.15$ in all cases, but the results are virtually invariant of the value chosen. We see that in more stratified stars the percentage of toroidal energy can increase, but the maximum toroidal field strength decreases with respect to the maximum poloidal field strength.

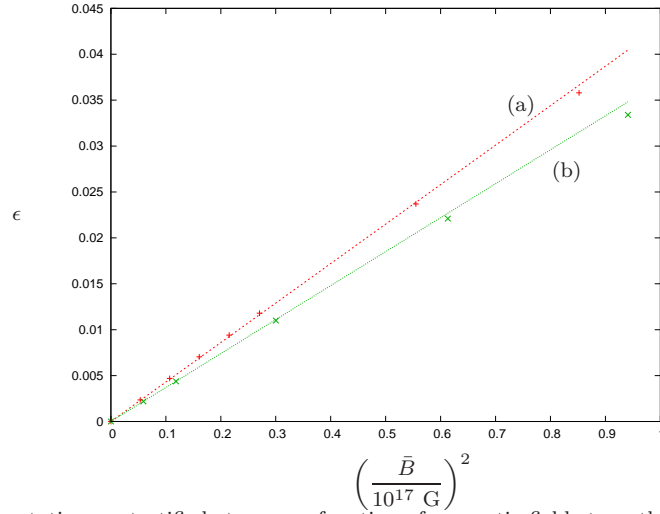


Figure 10. The ellipticity of nonrotating unstratified stars as a function of magnetic field strength. Line (a) shows the dependence for a poloidal field, whilst (b) shows a mixed-field configuration with 3% toroidal energy. The toroidal component decreases the oblateness of the star, as expected. There is no discernable difference in the corresponding figure for a stratified star; the ellipticity appears to be virtually independent of stratification.

6.3 Superconducting two-fluid equilibria with toroidal fields

In the previous section we investigated magnetic NS models with superfluid neutrons and normal protons. This situation could apply in (some) magnetars, if their interior magnetic fields exceed H_{c2} . Most NSs, however, are likely to be composed predominantly of superfluid neutrons and type-II superconducting protons. In this section we present the first NS models that account for this, specialising to configurations with purely toroidal magnetic fields.

In figure 11 we consider the variation of magnetic-field magnitude within the interior of two different NS models. The left-hand plot shows a star with normal protons and hence subject to the usual Lorentz force of MHD. It is also unstratified. The field strength is seen to drop off fairly slowly before vanishing at the stellar surface. In the right-hand plot we show a toroidal magnetic field in a superconducting star, with a particular choice of toroidal-field function which we refer to as ‘ ζ^3 -superconductivity’ — see section 3.2. This star is also stratified, and both this and the choice of toroidal-field function act to ‘bury’ the field deeper into the star. Our other choice for the toroidal-field function, ‘ ζ^2 -superconductivity’, produces configurations which are (in the unstratified case) indistinguishable from the left-hand plot. This is not surprising, since the expression for the toroidal field in this case is of the same form as for normal MHD (again, see section 3.2).

In figure 12 we show density distributions for three NS models with toroidal magnetic fields. We consider very highly magnetised stars, which serve to emphasise the magnetic distortions. All three models are broadly similar: each has a spherical

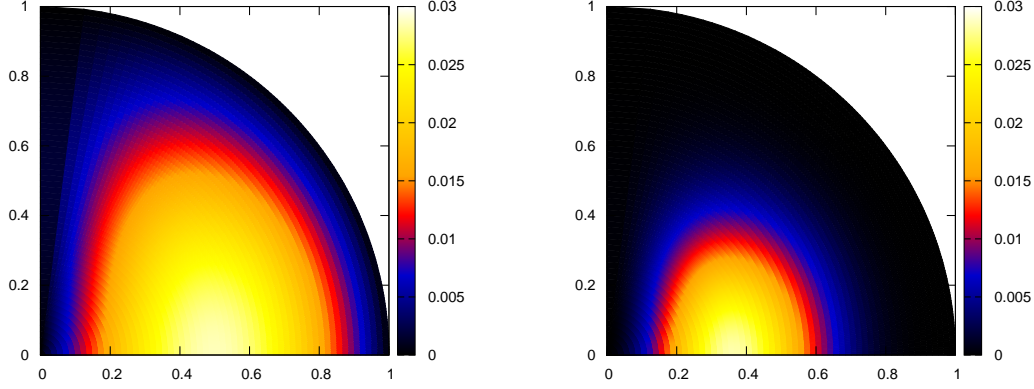


Figure 11. The variation in field strength within stars with purely toroidal magnetic fields. The left-hand plot shows a unstratified model in normal MHD; the right-hand plot shows ζ^3 -superconductivity in a stratified star. Both plots have the same maximum field strength, for easier comparison. Stratification and superconductivity both have the effect of concentrating the field in a smaller, more central region of the star.

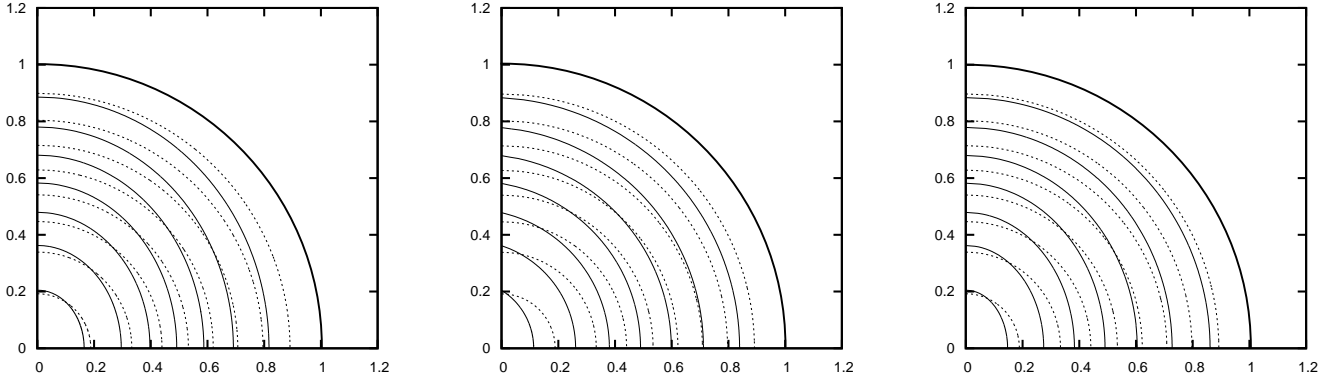


Figure 12. The distorting effect of a toroidal field. From left to right: normal MHD, ζ^2 -superconductivity, ζ^3 -superconductivity. The plots are all for very high field strengths (of the order of 10^{17} G), since the aim of the figure is to illustrate the different ways the density distribution is distorted in each case. We discuss more realistic values later.

neutron-fluid distribution, coincident neutron and proton-fluid surfaces, and prolate distortions of the proton fluid. Comparing the density contours for each model, we see that the superconducting models have less distortion to the proton fluid in the outer region, and more in the centre. The central panel (ζ^2 -superconductivity) has the unusual feature of cusps in its proton-fluid distribution around the pole. We show unstratified models, but the only obvious effect of stratification is that the spacing of the proton-fluid density contours is altered, as seen earlier in figure 7.

We mentioned that figure 12 shows models with extremely strong magnetic fields, and we will show models with similar field strengths in the next figure too. Whilst these high fields are useful for emphasising certain features, the main reason for using them comes from our numerical method, which calculates configurations based on a given distortion (axis ratio). Since magnetic distortions are typically very small, this means that even the axis ratio for the least non-spherical star we can specify (constrained by the grid resolution) corresponds to a very strong magnetic field. This is not necessarily a problem for normal MHD, but superconductivity will be broken at these field strengths, which exceed the second critical field of $H_{c2} \approx 10^{16}$ G. We are able to produce these models because the destruction of superconductivity is not built into them; the equations may be solved for any field strength. Having done so, however, we need to check that these models are consistent with our expectations for NSs with superconducting protons. If they are, we may extrapolate our results back to more realistic models, where $\bar{B} < \bar{H}_{c2}$.

We perform this sanity check next, in figure 13. We plot the scaling of ellipticity with average field strength \bar{B} for NS models with toroidal magnetic fields, for normal (left) and type-II superconducting protons (right). Note that all ellipticities are negative, since these configurations are prolate. In the left-hand plot we find that the measured numerical values agree very well with the expected scaling $\epsilon \propto B^2$, with small deviations when $\bar{B} \gtrsim 10^{17}$ G.

We now turn to the right-hand plot of figure 13. This time we plot the ellipticity against \bar{B} , not \bar{B}^2 . First we look at configurations with ζ^2 -superconductivity, for a central critical field value $H_{c1}(0) = 10^{16}$ G (the points on the line marked

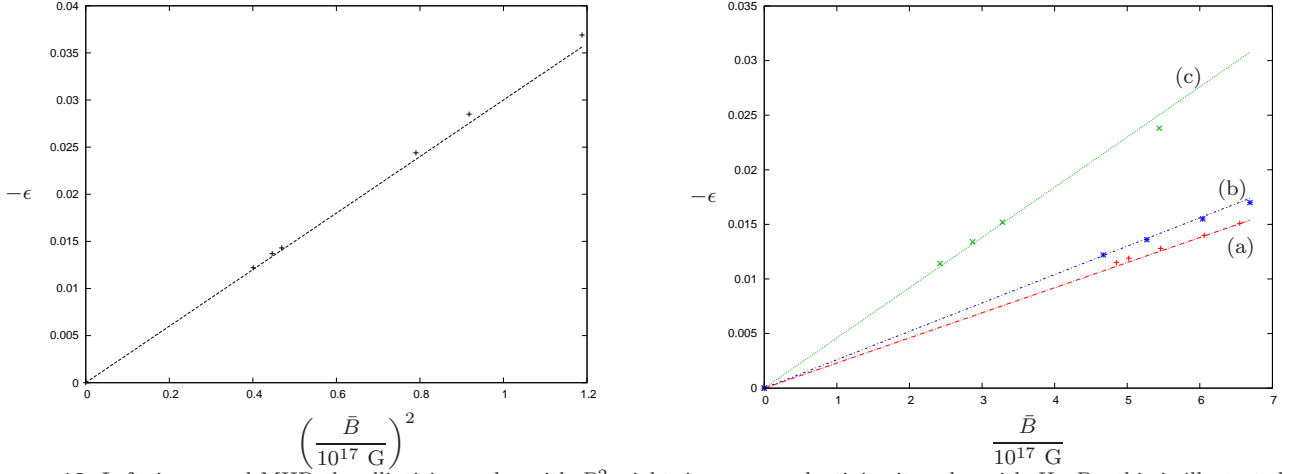


Figure 13. Left: in normal MHD the ellipticity scales with B^2 ; right: in superconductivity it scales with $H_{c1}B$ - this is illustrated by showing the results for a central critical-field value $H_{c1}(0) = 10^{16}$ G (a), and also $H_{c1}(0) = 2 \times 10^{16}$ G (c); the latter line has double the gradient. (a) and (c) are for ζ^2 -superconductivity; (b) is for ζ^3 -superconductivity with $H_{c1}(0) = 10^{16}$ G.

(a)) and also for $H_{c1}(0) = 2 \times 10^{16}$ G (the points on line (c)). In both cases we see that the points lie virtually on straight lines, showing that $\epsilon \propto \bar{B}$. In addition, line (c) has twice the gradient of line (a). This confirms that despite the high field strengths we are obliged to use (see the discussion above), we find the correct scaling of the ellipticity: $\epsilon \propto H_{c1}\bar{B}$. This gives us more confidence about our results and means we can safely extrapolate to more typical NS field strengths. We also present ellipticities for ζ^3 -superconductivity (points along line (b)). The level of distortion in this case is very similar to that in the ζ^2 case.

Note that for both plots in figure 13 we consider unstratified models, but we find that stratification makes no discernable difference to the ellipticity results. This is the same as for the previous plot showing ellipticities, figure 10.

6.4 Ellipticity formulae

In figures 10 and 13 we plotted ellipticities of two-fluid stars as a function of field strength for poloidal, toroidal and mixed fields in normal MHD, and toroidal fields in superconductivity. In all cases we found the scaling of points on the plots was in convincing agreement with the expected results: $\epsilon \propto \bar{B}^2$ in the normal case and $\epsilon \propto H_{c1}\bar{B}$ in superconductivity. In addition, for the very highest field strengths we were able to see slight deviations from this linear result. From the lines fitted to our data points we get quantitative relations between ellipticity and magnetic field strength, which we present here scaled to somewhat lower field strengths. In all cases the formulae are for two-fluid models without stratification, but we found that stratified stars obeyed the same relations, to a good approximation.

We begin with results for stars with superfluid neutrons and normal protons. In the case of purely toroidal fields we have

$$\epsilon = -3.0 \times 10^{-6} \left(\frac{\bar{B}}{10^{15} \text{ G}} \right)^2, \quad (66)$$

whilst for purely poloidal fields the relation is

$$\epsilon = 4.3 \times 10^{-6} \left(\frac{\bar{B}}{10^{15} \text{ G}} \right)^2. \quad (67)$$

We also consider mixed fields with 3% toroidal energy. This is relatively strong for our unstratified models, but still only produces a 14% reduction in oblateness from the purely poloidal case.

Next we consider models comprising superfluid neutrons and type-II superconducting protons with purely toroidal magnetic fields. As discussed in section 3.1, we have some flexibility in choosing the function η which governs the magnetic field. For our first choice of function, ζ^2 -superconductivity, we have

$$\epsilon = -2.3 \times 10^{-5} \left(\frac{H_{c1}(0)}{10^{16} \text{ G}} \right) \left(\frac{\bar{B}}{10^{15} \text{ G}} \right), \quad (68)$$

whilst for ζ^3 -superconductivity the relation is

$$\epsilon = -2.6 \times 10^{-5} \left(\frac{H_{c1}(0)}{10^{16} \text{ G}} \right) \left(\frac{\bar{B}}{10^{15} \text{ G}} \right). \quad (69)$$

We recall that these results were obtained using a density-dependent first critical field $H_{c1} = h_c \rho_p$, where h_c is a constant; in the above expressions we use the central critical field value $H_{c1}(0)$, normalised to 10^{16} G. The equivalent volume-averaged

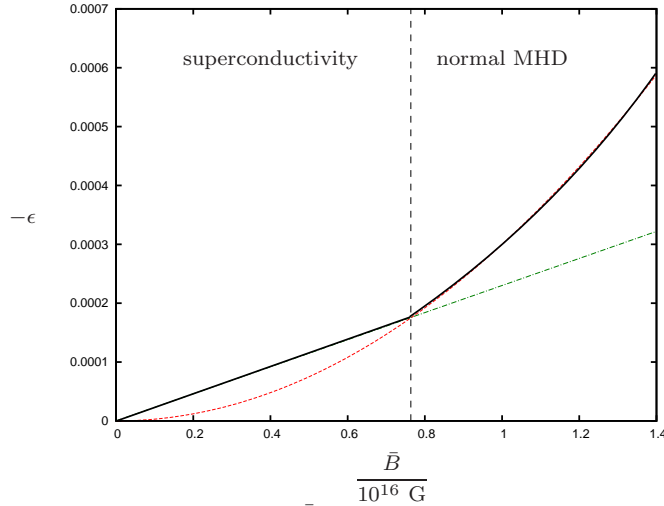


Figure 14. Below the (volume-averaged) second critical field \bar{H}_{c2} a NS has type-II superconducting protons and its ellipticity scales with $H_{c1}\bar{B}$ — considerably higher than the normal-MHD curve plotted below it. Above the critical field superconductivity is destroyed and the ellipticity has the normal-MHD scaling, quadratic in \bar{B} .

value is $\bar{H}_{c1} \approx 3 \times 10^{15}$ G. We note that the functional form of η has little effect on the ellipticity relation. The results in the superconducting case are in very good agreement with the barotropic study of Akgün & Wasserman (2008); using their ellipticity formula (71) gives a result just 5% different from our ζ^2 -superconductivity relation (68) and 15% different from (69).

We summarise these last two extrapolated formulae in figure 14, where we show the expected variation of ellipticity with field strength in a two-fluid NS model with a toroidal magnetic field. We assume that below the volume-averaged value of the second critical field $\bar{H}_{c2} \approx 10^{16}$ G the protons are superconducting, whilst above it they are normal. The neutrons are a superfluid in both cases. In the superconducting regime, $\epsilon \propto \bar{B}$ and the star is more distorted than one would expect from normal-MHD models. As the field strength is increased superconductivity is broken and the protons obey normal MHD, with $\epsilon \propto \bar{B}^2$.

Note that superconductivity can make a huge difference to the ellipticities predicted for most pulsars (Wasserman 2003); the discrepancy from normal MHD scales with \bar{H}_{c1}/\bar{B} . Let us take a pulsar with a volume-averaged field $\bar{B} = 10^{13}$ G, and assume this field is purely toroidal (since our only superconducting models are for this case). If the protons form a normal fluid we may apply equation (66) to predict that its ellipticity will be -3.0×10^{-10} ; if they are a type-II superconductor then equation (68) predicts that the ellipticity of the pulsar will be -2.3×10^{-7} — a factor of around 800 larger.

7 DISCUSSION

This paper, together with a companion paper Glampedakis, Andersson & Lander (2011), presents the first results on the equilibria of multifluid neutron stars with magnetic fields. Although it has been thought for decades that the fluid interiors of all but the youngest neutron stars are likely to comprise (predominantly) a neutron superfluid and a magnetised proton fluid, no previous studies have constructed equilibria of this kind. A related problem is the role of stratification in NSs. This renders the stellar matter non-barotropic and prevents the construction of single-fluid equilibria using the usual Grad-Shafranov equation (Reisenegger 2009). Virtually no studies have attempted to confront this extra difficulty; to our knowledge the only previous studies of magnetic equilibria in stratified stars are by Braithwaite — although these adopt an ideal-gas EOS more suited to main-sequence stars (Braithwaite & Nordlund 2006; Braithwaite 2009) — and the recent paper by Mastrano et al. (2011). Finally, in most neutron stars the protons are likely to form a type-II superconductor, which significantly changes the form of the magnetic force from the familiar Lorentz force. Once again, this effect has been neglected in most studies; the only related work on superconducting NS equilibria is that of Akgün & Wasserman (2008), although these are single-fluid models which do not have a separate neutron superfluid.

Within this paper we explore some of these issues. In the normal-MHD case, we show how the equations for a magnetised barotropic star may be generalised quite straightforwardly to a two-fluid model in which each fluid species obeys its own polytropic relation. By choosing different proton and neutron polytropic indices, we have a natural way of introducing stratification into the models. For simplicity we assume that all the stellar matter is multifluid, whereas NSs will also have regions which behave as a single fluid; when purely multifluid stars are better understood, it will be a logical future step to account for the effect of having these different fluid regions.

The equilibrium equations governing our stellar equilibria feature a number of apparently arbitrary magnetic functions, related to the strength of the magnetic field and its poloidal and toroidal field components. We argue that there are actually a number of restrictions on these functions, with little freedom in choosing them — and hence limited scope for producing qualitatively different equilibria from those we present here. Given this, we believe our results are quite generic to multifluid stars.

We also discuss the equations governing equilibria with type-II superconducting protons, starting from the relations derived in detail by Glampedakis, Andersson & Samuelsson (2011). The main difference from the normal-MHD two-fluid case is in the form of the magnetic force, which depends on the usual magnetic field \mathbf{B} but also on the first critical field H_{c1} , related to the presence of quantised fluxtubes. We use an approach inspired by the derivation of the Grad-Shafranov equation (see, e.g., Lander & Jones (2009)) to try to produce equilibrium equations that may be readily solved. As in the normal-MHD case, we arrive at a general equation governing the magnetic field, at which point one must specialise to different field configurations to get a solution. We remark that one important step from the normal-MHD derivation does not carry through to the superconducting case (and so may lead to significant differences between the two states), but we postpone a detailed discussion of this point to a later paper. For a purely toroidal magnetic field however, a solution may be obtained quite easily, so we specialise to this case in this paper.

In all cases, the equilibrium equations are solved numerically using an iterative procedure, which is a variation of the Hachisu SCF method (Hachisu 1986). This method is quite versatile and allows us to consider extremely strong magnetic fields, in contrast with the study reported in Glampedakis, Andersson & Lander (2011), where the magnetic field is regarded as a perturbation on a spherical background star. The good agreement between the results of this paper and Glampedakis, Andersson & Lander (2011), however, vindicate the latter work’s perturbative ansatz.

One main aim of this paper is to explore the role of stratification in a magnetised neutron star. We increase the stratification of the star by increasing the value of the proton-fluid polytropic index N_p , whilst fixing $N_n = 1$. For a purely poloidal field, this results in a larger closed-field line region, with the ‘neutral line’ (where the field strength vanishes) moving inwards; see figure 4. In mixed-field configurations the toroidal field component is contained in this region, and is consequently larger in stratified stars. Even in the stratified case, however, the energy in the poloidal component is always considerably greater than that in the toroidal component. This is because the parameter which increases the toroidal-component strength also *decreases* the size of the region occupied by this component (figure 5). These results are in good agreement with those of Glampedakis, Andersson & Lander (2011). Finally, for magnetic ellipticity relations our results suggest that stratification is not very important; there is little difference from the single-fluid barotropic relations.

We have not investigated the stability of any configurations presented here, although purely toroidal fields are unstable in both stratified and unstratified stars (Goossens & Tayler 1980), and it seems likely that the same will be true for purely poloidal fields, as in the unstratified case (Markey & Tayler 1973). This leaves mixed poloidal-toroidal fields as the only candidates for stable configurations, and hence the best models for NS magnetic fields. Although our configurations have quite small percentages of magnetic energy in the toroidal component, due to the small volume of the star it occupies, the magnitude of the two field components can be comparable. This suggests that these models could indeed be stable (Wright 1973). Note that Braithwaite (2009) suggested that a considerably higher percentage of toroidal-field energy was needed for stability. That work considered very different stellar models, however, more applicable to main-sequence stars than neutron stars. There is no consensus, as yet, about what percentages of each field component are likely to exist in real NSs.

Our other results concern equilibrium configurations of neutron stars with superfluid neutrons and type-II superconducting protons. In this initial study we specialise to purely toroidal magnetic fields, even though the equilibria we generate are likely to be unstable (Akgün & Wasserman 2008). From our results we are able to produce the first formulae for magnetic ellipticities of superconducting NSs based on a two-fluid model. Our results suggest that the distortion is around 50% greater than the estimate used by Cutler (2002) (having accounted for the fact that we also use a larger value for the critical field H_{c1}). There is very good agreement, however, with the ellipticity formula (equation 71) from Akgün & Wasserman (2008). If a substantial proportion of protons in a typical NS interior form a type-II superconductor, then ellipticity formulae based on models in normal MHD (e.g. Haskell et al. (2008) and Lander & Jones (2009)) greatly underestimate the potential magnetic distortion.

With the two-fluid model discussed in this paper, we are able to produce a wide range of different NS equilibria, accounting for stratification, superconductivity (with toroidal fields) and rotation. As well as being interesting in their own right, these equilibria could be used as background models on which to study perturbations. This would help us understand the stability of these various models, and their oscillation modes. The next logical step, however, is to consider superconducting stars with purely poloidal and mixed poloidal-toroidal magnetic fields. We hope to tackle this problem in a future study.

ACKNOWLEDGMENTS

SKL acknowledges funding from the European Science Foundation (ESF) for the activity entitled ‘The New Physics of Compact Stars’, NA acknowledges support from STFC in the UK through grant number ST/H002359/1 and KG is supported

by an Alexander von Humboldt fellowship and by the German Science Foundation (DFG) via SFB/TR7. We thank the referee Andreas Reisenegger for his detailed reading of this paper and useful criticism.

REFERENCES

- Akgün T., Wasserman I., 2008, MNRAS, 383, 1551
 Baym G., Pethick C., Pines D., 1969, Nature, 224, 673
 Braithwaite J., 2009, MNRAS, 397, 763
 Braithwaite J., Nordlund Å., 2006, A&A, 450, 1077
 Chandrasekhar S., 1961, *Hydrodynamic and Hydromagnetic Stability*, Clarendon, Oxford
 Cioffi R., Ferrari V., Gualtieri L., 2010, MNRAS, 406, 2540
 Cutler C., 2002, PRD, 66, 084025
 Dib R., Kaspi V.M., Gavril F.P., 2008, ApJ, 673, 1044
 Douchin F., Haensel P., 2001, A&A, 380, 151
 Easson I., 1979, ApJ, 228, 257
 Easson I., Pethick C.J., 1977, PRD, 16, 275
 Ferraro V.C.A., 1954, ApJ, 119, 407
 Glampedakis K., Andersson N., Lander S.K., 2011, arXiv:1106.6330
 Glampedakis K., Andersson N., Samuelsson L., 2011, MNRAS, 410, 805
 Goossens M., Tayler R.J., 1980, MNRAS, 193, 833
 Hachisu I., 1986, ApJS, 61, 479
 Harding A.K., Lai D., 2006, Rep. Prog. Phys., 69, 2631
 Haskell B., Samuelsson L., Glampedakis K., Andersson N., 2008, MNRAS, 385, 531
 Kaminker A.D., Haensel P., Yakovlev D.G., 2001, A&A, 373, L17
 Kaminker A.D., Yakovlev D.G., Potekhin A.Y., Shibasaki N., Shternin P.S., Gnedin O.Y., 2006, MNRAS, 371, 477
 Kiuchi K., Yoshida S., 2008, PRD, 78, 044045
 Lander S.K., Jones D.I., 2009, MNRAS, 395, 2162
 Markey P., Tayler R.J., 1973, MNRAS, 163, 77
 Mastrano A., Melatos A., Reisenegger A., Akgün T., 2011, arXiv:1108.0219
 Mendell G., 1991, ApJ, 380, 515
 Mereghetti S., 2008, A&AR, 15, 225
 Mestel L., 1956, MNRAS, 116, 324
 Ostriker J.P., Hartwick F.D.A., 1968, ApJ, 153, 797
 Ostriker J.P., Mark J.W.-K., 1968, ApJ, 151, 1075
 Page D., Prakash M., Lattimer J.M., Steiner A.W., 2011, PRL, 106, 081101
 Passamonti A., Haskell B., Andersson N., 2009, MNRAS, 396, 951
 Prix R., Comer G.L., Andersson N., 2002, A&A, 381, 178
 Prix R., Novak J., Comer G.L., 2005, PRD, 043005
 Prix R., Rieutord M., 2002, A&A, 393, 949
 Reisenegger A., 2009, A&A, 499, 557
 Reisenegger A., Goldreich P., 1992, ApJ, 395, 240
 Roxburgh I., 1966, MNRAS, 132, 347
 Shternin P.S., Yakovlev D.G., Heinke C.O., Ho W.C.G., Patnaude D.J., 2011, MNRAS, 412, L108
 Tomimura Y., Eriguchi Y., 2005, MNRAS, 359, 1117
 Wasserman I., 2003, MNRAS, 341, 1020
 Wright G.A.E., 1973, MNRAS, 162, 339
 Yoshida S., Eriguchi Y., 2004, MNRAS, 347, 575